

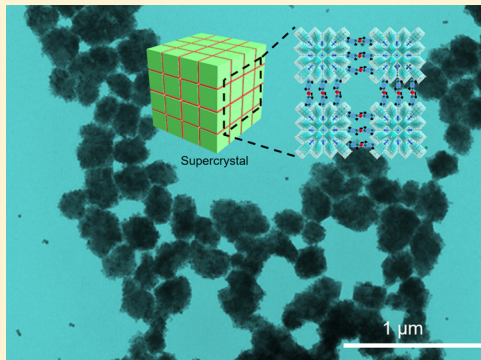
# Metal Halide Perovskite Supercrystals: Gold–Bromide Complex Triggered Assembly of $\text{CsPbBr}_3$ Nanocubes

Kun-Hua Wang,<sup>†,‡</sup> Jun-Nan Yang,<sup>‡</sup> Qian-Kun Ni,<sup>‡</sup> Hong-Bin Yao,<sup>\*,†,‡,§,||,⊥,ID</sup> and Shu-Hong Yu<sup>\*,†,‡,§,||,⊥,ID</sup>

<sup>†</sup>Division of Nanomaterials & Chemistry, Hefei National Laboratory for Physical Sciences at Microscale, <sup>‡</sup>Department of Chemistry, <sup>§</sup>CAS Center for Excellence in Nanoscience, <sup>||</sup>Hefei Science Center of CAS, and <sup>⊥</sup>Collaborative Innovation Center of Suzhou Nano Science and Technology, University of Science and Technology of China, Hefei, Anhui 230026, P. R. China

## S Supporting Information

**ABSTRACT:** Using nanocrystals as “artificial atoms” to construct supercrystals is an interesting process to explore the stacking style of nanoscale building blocks and corresponding collective properties. Various types of semiconducting supercrystals have been constructed via the assembly of nanocrystals driven by the entropic, electrostatic, or van der Waals interactions. We report a new type of metal halide perovskite supercrystals via the gold–bromide complex triggered assembly of newly emerged attractive  $\text{CsPbBr}_3$  nanocubes. Through introducing gold–bromide ( $\text{Au}–\text{Br}$ ) complexes into  $\text{CsPbBr}_3$  nanocubes suspension, the self-assembly process of  $\text{CsPbBr}_3$  nanocubes to form supercrystals was investigated with the different amount of  $\text{Au}–\text{Br}$  complexes added to the suspensions, which indicates that the driven force of the formation of  $\text{CsPbBr}_3$  supercrystals included the van der Waals interactions among carbon chains and electrostatic interactions between  $\text{Au}–\text{Br}$  complexes and surfactants. Accordingly, the optical properties change with the assembly of  $\text{CsPbBr}_3$  nanocubes and the variation of mesoscale structures of supercrystals with heating treatment was revealed as well, demonstrating the ionic characteristics of  $\text{CsPbBr}_3$  nanocrystals. The fabricated  $\text{CsPbBr}_3$  supercrystal presents a novel type of semiconducting supercrystals that will open an avenue for the assembly of ionic nanocrystals.



## INTRODUCTION

Three-dimensional (3D) self-assemblies of nanocrystals (NCs) to form superlattices or supercrystals are of great interest for the development of advanced materials with potential applications in field-effect transistors,<sup>1</sup> light-emitting diodes,<sup>2</sup> plasmonic waveguides,<sup>3</sup> magnetic recording media,<sup>4</sup> and so on. Previous studies of the assembly of NCs have shown that the assembled supercrystals are highly related to the shapes of nanoscale building blocks and the interactions among the building blocks.<sup>5–7</sup> In general, spherical NCs self-assembled into hexagonal close-packed structures or face-centered cubic to perform the highest packing efficiency, that is, 74.04%.<sup>8–10</sup> Nanocubes with flat faces and sharp edges prefer to assemble in simple cubic superlattices.<sup>11–13</sup> Diverse types of supercrystals have been obtained via the assembly of nanocubes due to the high face-to-face interactions among nanocubes.<sup>14–17</sup> These reported 3D supercrystals consisting of single- or multicomponent NCs are routinely achieved by the self-assembly processes induced by entropic, electrostatic, or van der Waals interactions.<sup>18–20</sup>

Very recently, metal halide perovskite NCs have attracted intensive attention due to their unique properties including high photoluminescence (PL), anion-exchange tuning optical band gaps, and narrow emissions.<sup>21–25</sup> A series of metal halide perovskite NCs have been synthesized and have shown intriguing properties.<sup>26–31</sup> In particular, monodisperse colloidal  $\text{CsPbBr}_3$  NCs with well-defined nanocube shapes have been synthesized

and exhibited bright emission with wide color gamut.<sup>28,32</sup> In addition, fast anion-exchange performance has also been reported in metal halide perovskite NCs.<sup>33–36</sup> These newborn nanomaterials will be interesting nanoscale building blocks to study the assembly process of nanostructures due to their high PL, well-defined cube shape, and ionic polar surfaces. However, the self-assembly of colloidal  $\text{CsPbBr}_3$  nanocubes to form supercrystals and their collective properties are rarely reported.<sup>37,38</sup>

Distinctive from traditional semiconductors, metal halide perovskites possess not only the properties of classical semiconductors but also the complex defect physics of ionic crystals. Compared with typical metal chalcogenides, such as ternary ( $\text{CuInS}_2$  and  $\text{AgInS}_2$ ) compounds, ternary  $\text{CsPbBr}_3$  NCs have high ionic conductivities<sup>28</sup> and the fast speed of anion-exchange in perovskite NCs, which is rooted from the ionic properties of perovskite metal halide crystals.<sup>34</sup> The highly ionic character of  $\text{CsPbBr}_3$  nanocubes would bring a new viewpoint for the 3D supercrystals assemblies of ionic NCs.

We report a new type of 3D supercrystals based on the self-assembly of  $\text{CsPbBr}_3$  nanocubes triggered by  $\text{Au}–\text{Br}$  complexes via the van der Waals interactions and electrostatic forces, in which the electrostatic forces between  $\text{Au}–\text{Br}$  complexes and

Received: October 1, 2017

Revised: December 16, 2017

Published: December 18, 2017

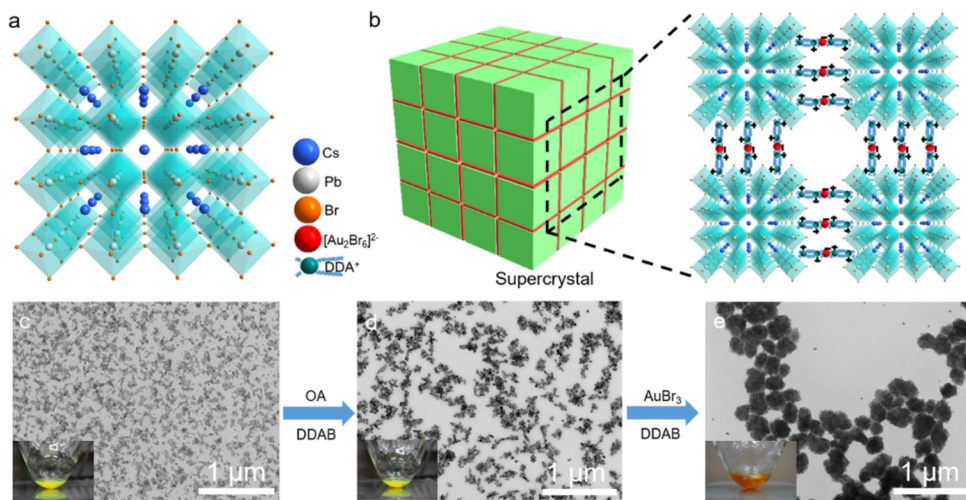


**Figure 1.** (a) Crystal structural model of cubic CsPbBr<sub>3</sub>. (b) Illustration of the formation mechanism of supercrystals. (c) TEM image of as-synthesized CsPbBr<sub>3</sub> nanocubes (inset: the photo of as-synthesized CsPbBr<sub>3</sub> nanocube suspension). (d) TEM image of ligand-exchanged CsPbBr<sub>3</sub> nanocubes (inset: the photo of ligand-exchanged CsPbBr<sub>3</sub> nanocube suspension). (e) TEM image of assembled CsPbBr<sub>3</sub> nanocubes (inset: the photo of assembled CsPbBr<sub>3</sub> nanocube suspension).

surfactants played an important role in the formation of 3D supercrystals. The size and quantity of as-fabricated super-crystals have been demonstrated to be tunable by varying the amount of Au–Br complexes added to the CsPbBr<sub>3</sub> nanocubes suspension. Extensive nanoscale structural characterizations revealed that a different number of faces on the CsPbBr<sub>3</sub> nanocubes could interact with each other via the van der Waals and electrostatic interactions. During the assembly process the quenching of PL of CsPbBr<sub>3</sub> nanocubes was observed, which is related to the aggregation of nanocubes and the introduction of trap states on the surfaces of CsPbBr<sub>3</sub> nanocubes by Au–Br complexes. More interestingly, the obtained CsPbBr<sub>3</sub> supercrystals preferred to form mesocrystals rather than disassembling into individual nanocubes after a heat treatment at 80 °C, indicating the inherently active ionic properties of CsPbBr<sub>3</sub> nanocubes.

## EXPERIMENTAL SECTION

**Materials and Chemicals.** Lead bromide (PbBr<sub>2</sub>, Afla Aesar, 98%), oleic acid (OA, Sinopharm Chemical Reagent (SCRC), AR), oleylamine (OAm, Aldrich, 70%), gold bromide (AuBr<sub>3</sub>, Aladdin, 99%), toluene (C<sub>7</sub>H<sub>8</sub>, SCRC, AR), 1-butanol (BuOH, SCRC, AR), octadecene (ODE, Aldrich, 90%), cesium carbonate (Cs<sub>2</sub>CO<sub>3</sub>, 99.9%, J&K), didodecyldimethylammonium bromide (DDAB, 98%, J&K), and hexane (C<sub>6</sub>H<sub>14</sub>, SCRC, AR) were used as received without further purification.

**Preparation of Cs-Oleate.** Cs<sub>2</sub>CO<sub>3</sub> (0.814 g) was loaded into a 100 mL three-necked flask along with ODE (40 mL) and OA (2.5 mL), dried for 1 h at 120 °C, and then heated under N<sub>2</sub> to 150 °C until all Cs<sub>2</sub>CO<sub>3</sub> reacted with OA. Because Cs-oleate precipitates out from ODE at room temperature, it must be preheated to 100 °C before the following injection process.

**Synthesis and Purification of CsPbBr<sub>3</sub>.** PbBr<sub>2</sub> (0.035g) and ODE (5 mL) were loaded into a 25 mL three-necked flask and dried under vacuum at 120 °C for 30 min. Then, OA (0.5 mL) and OAm (0.5 mL) were injected into the three-necked flask at 120 °C under N<sub>2</sub> flow. After complete dissolution of PbBr<sub>2</sub> in ODE, the temperature was raised to 180 °C and Cs-oleate ODE solution (0.2 mL) was swiftly injected and 1 min later the reaction mixture was cooled by ice–water bath. The crude solution was precipitated by BuOH before centrifugation and then purified with toluene at 12 000 rpm for 3 min. The final precipitate was redispersed in 5 mL of hexane for further use.

**Assembly of CsPbBr<sub>3</sub> into Supercrystals.** The Au–Br complex solution was prepared containing 0.01 g of AuBr<sub>3</sub> (0.024 mmol) and

0.01 g of DDAB (0.024 mmol) in 4 mL of toluene and vibrated for 10 min at room temperature. AuBr<sub>3</sub> was easily dissolved in the toluene/DDAB mixture, forming a clear dark-orange solution. 50 μL of OA and 100 μL of DDAB toluene solution (0.01 M) were added to 2.5 mL of as-prepared hexane suspension of CsPbBr<sub>3</sub> solution under vigorous stirring, respectively; then, a desired amount of DDAB–AuBr<sub>3</sub> solution was added to the CsPbBr<sub>3</sub> suspension to trigger the assembly of CsPbBr<sub>3</sub> NCs into supercrystals. The assembly process was carried out under a N<sub>2</sub> atmosphere. After 20 min of stirring for assembly the assembled sample was collected by centrifugation at 12 000 rpm.

**Heating Treatment of the Assembled CsPbBr<sub>3</sub> Supercrystals.** The obtained assembled CsPbBr<sub>3</sub> supercrystals were redispersed in 2.5 mL of toluene, heated to 80 °C for 30 min under a N<sub>2</sub> atmosphere, and then collected by centrifugation at 12 000 rpm.

**Characterizations.** *Transmission Electron Microscope.* Transmission electron microscope (TEM) images were acquired on a Hitachi HT-7700 transmission electron microscope with an accelerating voltage of 120 kV. High-angle annular dark-field scanning transmission electron microscopy (HAADF-STEM), high-resolution TEM (HRTEM) images, and the energy-dispersive spectra (EDS) were acquired on a Jeol JEM-2100F transmission electron microscope at an accelerating voltage of 200 kV equipped with an energy-dispersive detector.

**Optical Properties Characterization.** UV–visible absorption spectra were collected by using a PekinElmer in transmission mode. The PL spectra and PLQYs were taken by a Hamamatsu absolute PL yield spectrometer C11347.

**X-ray Photoelectron Spectroscopy.** X-ray photoelectron spectroscopy (XPS) of selected samples were recorded on an ESCALAB 250.

**X-ray Diffraction Measurements.** Powder X-ray diffraction (XRD) was measured using a Philips X’Pert PRO SUPER X-ray diffractometer equipped with graphite monochromatized Cu K $\alpha$  radiation.

**Inductively Coupled Plasma-Mass Spectrometry.** Molar ratios of Cs, Br, Pb, and Au were measured through inductively coupled plasma-mass spectrometry (ICP-MS) on an Optima 7300 DV apparatus.

**Proton Nuclear Magnetic Resonance Measurements.** Proton nuclear magnetic resonance (<sup>1</sup>H NMR) measurements were recorded on a Bruker Avance III HD spectrometer operating at a <sup>1</sup>H frequency of 400 MHz and equipped with a BBFO-Z probe.

**Thermal Gravimetric Analysis.** Thermal gravimetric analysis (TGA) was performed under a N<sub>2</sub> atmosphere on a SDT Q600 TGA instrument using a heating rate of 10 °C/min to a temperature of 900 °C.

## RESULTS AND DISCUSSION

The ionic CsPbBr<sub>3</sub> nanocubes present a different assembly style comparing to traditional semiconductor NCs on the atomic

scale. As shown in Figure 1a, the cubic phase of  $\text{CsPbBr}_3$  behaves as a 3D connected structure, in which the octahedral coordination of  $\text{Pb}^{2+}$  with six  $\text{Br}^-$  extends to three dimensions via sharing the vertex and  $\text{Cs}^+$  ions localize in the octahedral voids. In this 3D ionic crystal structure, bromide anions can be easily extracted and replaced by other halides due to their single ionic charge, the rigid nature of the cationic sublattice, as well as an efficient vacancy-assisted diffusion mechanism.<sup>34</sup> In addition, from a structural standpoint, the exposure of rich  $\text{Br}^-$  on the surface of  $\text{CsPbBr}_3$  NCs makes it feasible to give rise to strong affinity with positive surfactants.<sup>39</sup> Figure 1b illustrates the proposed driven force for the assembly of  $\text{CsPbBr}_3$  NCs triggered by  $\text{Au}-\text{Br}$  complexes, for example, van der Waals interactions among carbon chains and electrostatic forces between  $\text{Au}-\text{Br}$  complexes and surfactants. In particular, the electrostatic forces between  $\text{Au}-\text{Br}$  complexes and positively charged surfactants would play the key role in the assembly of  $\text{CsPbBr}_3$  NCs. The interactions between these  $\text{CsPbBr}_3$  nanocubes result in the face-to-face contact, which further induces the formation of 3D supercrystals.

To trigger the assembly of  $\text{CsPbBr}_3$  nanocubes into supercrystals, the ligand exchange and the addition of  $\text{Au}-\text{Br}$  complexes into the  $\text{CsPbBr}_3$  nanocube suspension were carried out in a sequent process, as shown in Figure 1c–e. Typically, the  $\text{CsPbBr}_3$  nanocubes were first synthesized according to the literature<sup>34</sup> and dispersed into the hexane forming the suspension (1.6 mg/mL) (inset in Figure 1c). In this suspension, the  $\text{CsPbBr}_3$  nanocubes are monodisperse and only form the small monolayer aggregations on the TEM grid after the evaporation of hexane (Figure 1c). Then, 50  $\mu\text{L}$  of oleic acid (OA) and 100  $\mu\text{L}$  of didodecyldimethylammonium bromide (DDAB, 0.01 M) solution in toluene were added to 2.5 mL of as-prepared hexane suspension of  $\text{CsPbBr}_3$  nanocubes under stirring to further improve the dispersion of nanocubes in the solvent via the ligand-exchange role of DDAB.<sup>40</sup> After the ligand exchange, the color of suspension still remained bright

green (Inset in Figure 2d) and the transparency and PL intensity were enhanced (Supporting Information, Figure S1) indicating the improved dispersion of  $\text{CsPbBr}_3$  nanocubes in the solvent induced by the ligand exchange. Similarly, the ligand-exchanged  $\text{CsPbBr}_3$  nanocubes still only formed the monolayer aggregations on the TEM grid after the evaporation of solvent (Figure 1d). Finally, 1 mL of DDAB– $\text{AuBr}_3$  solution (0.006 M) in toluene was injected into the ligand-exchanged  $\text{CsPbBr}_3$  suspension to induce the assembly of monodisperse  $\text{CsPbBr}_3$  nanocubes, with the color change of suspension from yellow to orange (inset in Figure 1e). TEM image of the assembled  $\text{CsPbBr}_3$  nanocubes (Figure 1e) clearly shows that the nanocubes stacked together into cubic superstructures with the size of ~300 nm after the addition of 1 mL of DDAB– $\text{AuBr}_3$  solution into the  $\text{CsPbBr}_3$  suspension. Furthermore, the assembled  $\text{CsPbBr}_3$  nanocubes still maintain cubic phase without any phase change (Figure S2).

To show the role of  $\text{Au}-\text{Br}$  complexes on the self-assembly of  $\text{CsPbBr}_3$  nanocubes, we further investigated the influence of the amount of DDAB– $\text{AuBr}_3$  solution on the self-assembly behaviors of  $\text{CsPbBr}_3$  nanocubes. We first confirmed that the 1:1 molar ratio of DDAB– $\text{AuBr}_3$  is key for triggering the self-assembly, and other ratios including 2:1 and 1:2 are unable to enable the assembly of  $\text{CsPbBr}_3$  nanocubes (Figure S3). Then, a series amount of DDAB– $\text{AuBr}_3$  (1:1) toluene solution was added to the  $\text{CsPbBr}_3$  nanocubes suspensions, respectively, to investigate the effect of  $\text{Au}-\text{Br}$  complexes on the assembly of  $\text{CsPbBr}_3$  nanocubes. With increasing the amount of DDAB– $\text{AuBr}_3$  solution added to the  $\text{CsPbBr}_3$  nanocubes suspension, the assemblies of nanocubes changed from 2D square arrays to 3D simple cubic superlattices. Figure 2a,b shows that when 0.1 and 0.2 mL of DDAB– $\text{AuBr}_3$  solution are added to the  $\text{CsPbBr}_3$  nanocubes suspension, respectively, each of these nanocubes is surrounded by four others, forming 2D square arrays. As shown in Figure 2c, with the addition of 0.3 mL of DDAB– $\text{AuBr}_3$  solution into the  $\text{CsPbBr}_3$  nanocube suspension, more nanocubes were gradually aggregated and all six faces of each

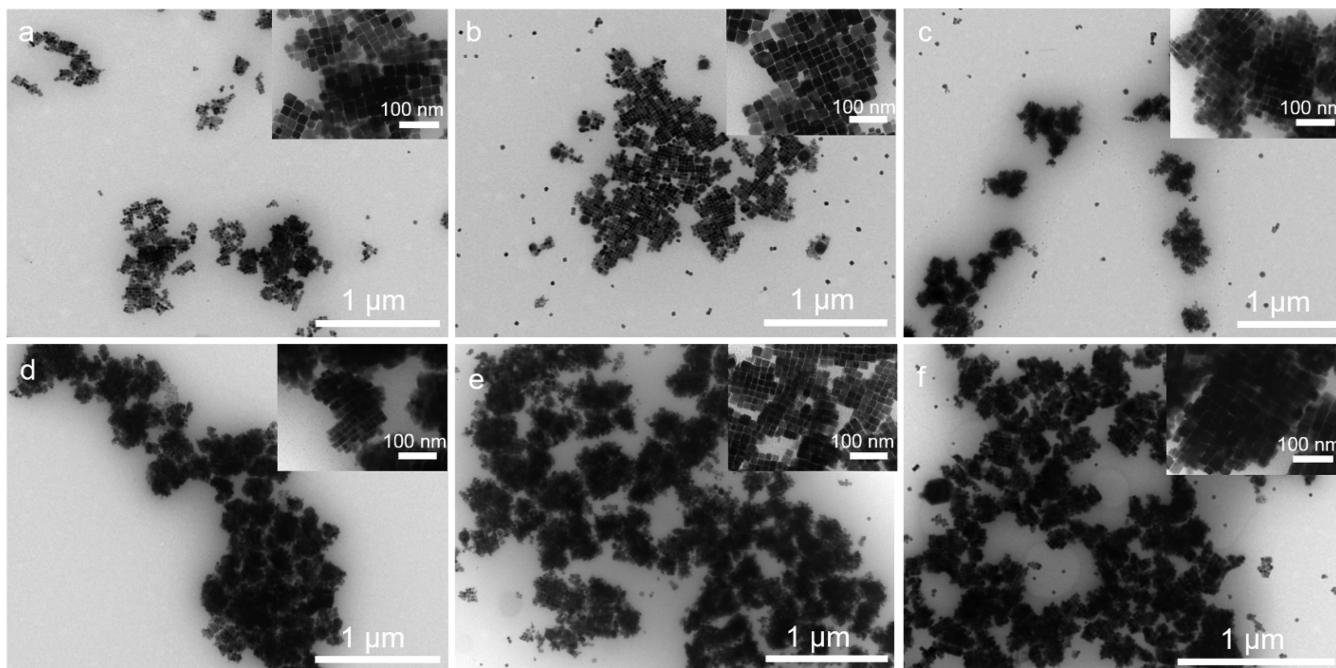


**Figure 2.** (a–f) TEM images of assembled  $\text{CsPbBr}_3$  nanocubes with addition of different amount of DDAB– $\text{AuBr}_3$  solution: 0.1, 0.2, 0.3, 0.4, 1, and 1.5 mL, respectively.

nanocube interacted with other nanocubes, forming 3D superlattices. Figure 2d–e demonstrates that the size of assemblies increased with increasing the amount of DDAB–AuBr<sub>3</sub> solution from 0.4 to 1 mL. However, as shown in Figure 2f, the size would not further increase even if the amount of DDAB–AuBr<sub>3</sub> solution increased to 1.5 mL. The size variation of assembled CsPbBr<sub>3</sub> supercrystals with the increase in amount of DDAB–AuBr<sub>3</sub> solution added to the suspension is plot in Figure S4, which indicates that the size of supercrystals reached a saturated value when the amount of DDAB–AuBr<sub>3</sub> solution increased to 1 mL due to the balance of assembly and disassembly of CsPbBr<sub>3</sub> nanocubes around the supercrystals. Furthermore, we compared the size of as-synthesized single CsPbBr<sub>3</sub> nanocube and the CsPbBr<sub>3</sub> nanocube in the assembled supercrystal. As shown in Figure S5, the size distribution of initially synthesized single CsPbBr<sub>3</sub> NC before assembly indicated that the size of most CsPbBr<sub>3</sub> nanocubes (75%) was in the range of 13–17 nm. Figure S5b–g show that the sizes of most of single CsPbBr<sub>3</sub> particles (75%) in the assembled supercrystals were in the range of 16–24 nm, which is possibly caused by the size variation of CsPbBr<sub>3</sub> NCs synthesized at different batches. Moreover, we also synthesized CsPbBr<sub>3</sub> nanocubes with smaller size (75%, 10–13 nm) as initial building blocks to conduct the assembly. As shown in Figure S6, the assembled CsPbBr<sub>3</sub> supercrystals with the addition of different amount of DDAB–AuBr<sub>3</sub> solution can be obtained as well. The results indicate that the assembly behavior of CsPbBr<sub>3</sub> NCs could be achieved at relatively smaller sizes as well. In addition, the size distribution statistics (insets in Figure S6) indicate that the sizes of most (75%) of single CsPbBr<sub>3</sub> nanocubes after assembly are in the range of 10–15 nm.

To reveal the dominate role of Au–Br complexes for the formation of CsPbBr<sub>3</sub> supercrystals, we further studied other interactions that possibly existed in the self-assembly process of CsPbBr<sub>3</sub> nanocubes. To illustrate that only dipole–dipole interactions of DDAB could not be enough to intrigue the formation of 3D CsPbBr<sub>3</sub> supercrystals, the same amount of DDAB solution without AuBr<sub>3</sub> was added to the CsPbBr<sub>3</sub> nanocubes suspension and the other conditions were kept the same. Figure S7 shows that the CsPbBr<sub>3</sub> nanocubes failed to assemble into 3D supercrystals, indicating that the assembly force of CsPbBr<sub>3</sub>

nanocubes could not only be attributed to the entropic force of DDAB, indicating that the electrostatic interactions between Au–Br complexes and surfactants is indispensable. To reveal the possible electrostatic force among the CsPbBr<sub>3</sub> nanocubes for the formation of superlattices, we also measured the zeta potentials of as-synthesized CsPbBr<sub>3</sub> nanocubes, ligand-exchanged CsPbBr<sub>3</sub> nanocubes, and assembled CsPbBr<sub>3</sub> supercrystals, respectively. The results were summarized in Table S1. Similar to a negative value of −3.98 mV for the zeta potential of pristine CsPbBr<sub>3</sub> nanocubes, ligand-exchanged CsPbBr<sub>3</sub> nanocubes also show a negative zeta potential of −4.92 mV, which is consistent with previous report.<sup>40</sup> This negative zeta potential facilitated the adsorption of positive charged ligands, DDA<sup>+</sup>, on the surface of CsPbBr<sub>3</sub> nanocubes, which acted as the bridges to connect the CsPbBr<sub>3</sub> nanocubes together under the help of Au–Br complexes. In addition, the zeta potential of finally assembled CsPbBr<sub>3</sub> supercrystals is still negative (−6.48 mV), implying that the Br<sup>−</sup> always remained rich on the surface of CsPbBr<sub>3</sub> nanocubes, confirming the ionic characteristics of CsPbBr<sub>3</sub>.

To verify the existence of Au–Br complexes among the assembled CsPbBr<sub>3</sub> nanocubes to induce the formation of supercrystals and specifically describe the Au–Br complexes, we comprehensively characterized the CsPbBr<sub>3</sub> supercrystals by HAADF-STEM, EDS, and X-ray photoelectron spectroscopy (XPS). Figure 3a shows the TEM image of well-defined CsPbBr<sub>3</sub> supercrystals obtained by adding 1 mL of DDAB–AuBr<sub>3</sub> solution to CsPbBr<sub>3</sub> suspension, which indicates that CsPbBr<sub>3</sub> NCs were tightly connected face-to-face with each other, forming the well-defined supercrystals. Figure 3b displays the corresponding HAADF-STEM image, also showing the uniform supercrystals assembled by the CsPbBr<sub>3</sub> NCs and maintaining the consistency with the EDS mappings. As shown in Figure 3c–f, the EDS mappings of Pb, Au, and Br overlapped very well, which indicates that Au element is homogeneously dispersed in the whole supercrystals. In addition, the signal intensity of Br is much stronger than that of Pb, indicating that the Au–Br complexes acted as the main forms to connect the CsPbBr<sub>3</sub> NCs. Meanwhile, the low content of Au in the supercrystals is consistent with the small amount of Au–Br complex added to the CsPbBr<sub>3</sub> nanocube suspension. For comparison, we also

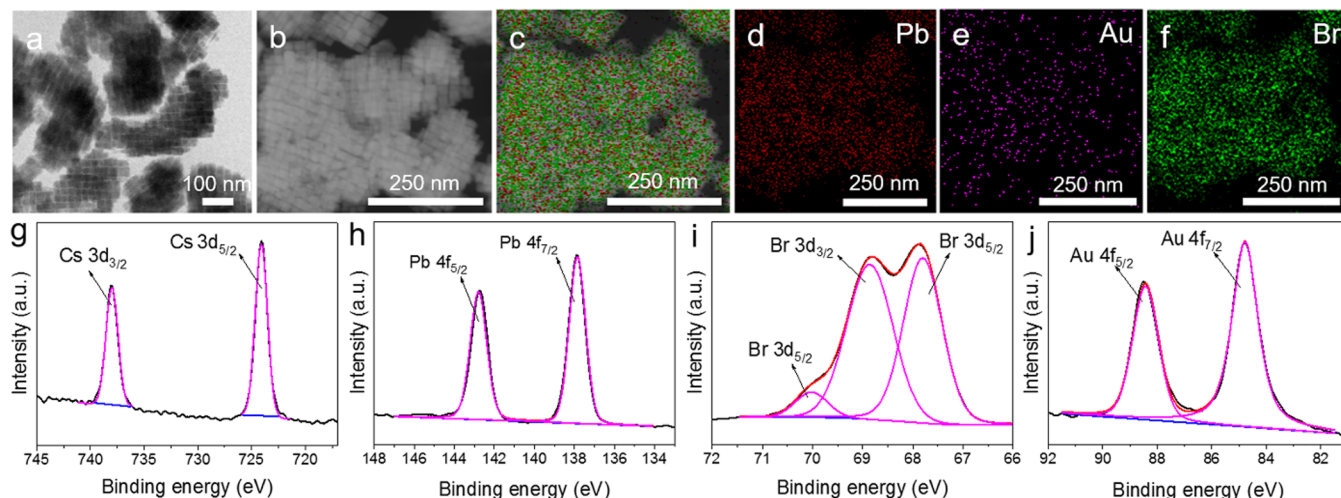


**Figure 3.** (a) TEM image of assembled CsPbBr<sub>3</sub> nanocubes by adding 1 mL of DDAB–AuBr<sub>3</sub> solution into the CsPbBr<sub>3</sub> suspension. (b) Corresponding HAADF-STEM image of assembled CsPbBr<sub>3</sub> nanocubes. (c–f) EDS mappings of assembled CsPbBr<sub>3</sub> nanocubes. (g–j) XPS spectra of assembled CsPbBr<sub>3</sub> nanocubes for the Cs (3d), Pb (4f), Br (3d), and Au (4f) as marked in corresponding curves, respectively.

used XPS to characterize the  $\text{CsPbBr}_3$  nanocubes before the addition of Au–Br complexes, the results of which are shown in Figure S8. As we can see, all elements (Cs, Pb, and Br) can be detected due to the pure phase of as-synthesized  $\text{CsPbBr}_3$  nanocubes. In particular, the Br 3d binding energy curve for  $\text{CsPbBr}_3$  nanocubes before the addition of Au–Br complex can be fitted to only two peaks at 69.15 and 68.1 eV. After the addition of Au–Br complexes to trigger the assembly of  $\text{CsPbBr}_3$  nanocubes, besides the Cs, Pb, and Br, the Au element can be detected, as shown in Figure 3g–j. The binding energy curve of Au 4f can be fitted into two peaks at 88.5 and 84.8 eV, indicating the existence of Au–Br complex ( $[\text{Au}_2\text{Br}_6]^{2-}$ ) in the assembled supercrystals. More interestingly, the Br 3d core level of  $\text{CsPbBr}_3$  nanocubes after the addition of Au–Br complexes can be fitted into three peaks at 70, 68.8, and 67.8 eV, indicating the existence of Br–Br bridge bonding in the assembled samples.

To reveal the ratio of components in the assembled supercrystals, we used the ICP-MS,  $^1\text{H}$  NMR (Figures S9–S12), and TGA (Figure S13) to analyze the compositions including inorganic and organic parts in the supercrystals. For the inorganic part, we performed ICP-MS to determine the molar ratio of Cs/Br/Pb/Au is 1.1:3.2:1:0.03 in assembled  $\text{CsPbBr}_3$  supercrystals with the addition of 0.5 mL of DDAB– $\text{AuBr}_3$  solution. When assembling  $\text{CsPbBr}_3$  NCs with the addition of 1 mL of DDAB– $\text{AuBr}_3$  solution, the molar ratio of Cs/Br/Pb/Au in the obtained supercrystals is 1.01:3.1:1:0.06. The ICP-MS results show that the ratio of Cs/Br/Pb varied little in the assembled samples obtained by adding different amount of DDAB– $\text{AuBr}_3$  solution, but the ratio of Pb/Au increased with the amount of DDAB– $\text{AuBr}_3$  added to the assembly solution. This means that  $\text{CsPbBr}_3$  nanocubes were stable during the assembly, and higher concentration of DDAB– $\text{AuBr}_3$  solution induced more Au complexes embedded in the obtained supercrystals. For the organic part, we used  $^1\text{H}$  NMR to study the variation of ligands on the surface of  $\text{CsPbBr}_3$  nanocubes before and after assembly. Compared with the reference spectrum of 1-octadecene (ODE), oleic acid (OA), oleylamine (OAm), and DDA $^+$  (Figure S9), Figure S10 clearly shows the characteristic resonances of ODE, OA and OAm in  $\text{CsPbBr}_3$  nanocubes, and their ratio was determined to be 5.3:2.7:2.0 according to integral area of specific  $^1\text{H}$  NMR peaks. After adding 0.5 mL of DDAB– $\text{AuBr}_3$  solution to trigger the assembly of  $\text{CsPbBr}_3$  nanocubes, only OA and DDA $^+$  can be detected, as shown in Figure S11, and their ratio is 8.9:1.1. Similarly, after adding 1 mL of DDAB– $\text{AuBr}_3$  solution to trigger the assembly of  $\text{CsPbBr}_3$  nanocubes, the amount of OA declined and the DDA $^+$  increased, and their ratio is 8.5:1.5 (Figure S12). The  $^1\text{H}$  NMR results indicate that with the assembly processing, DDA $^+$  gradually replaces OA and OAm to conduct the assembly of  $\text{CsPbBr}_3$  nanocubes due to the stronger affinity of DDA $^+$  with the Br $^-$  on the surface of nanocubes. In accordance with integrally weak peaks in  $^1\text{H}$  NMR, TGA (Figure S13) also indicates that the content of organic component is only 8.9 wt % in the assembled  $\text{CsPbBr}_3$  supercrystals with the addition of 1 mL of DDAB– $\text{AuBr}_3$  solution. In the combination of all of the above analysis, the formula of assembled supercrystals with the addition of 1 mL of DDAB– $\text{AuBr}_3$  solution was determined to be  $(\text{OA})_{0.159}(\text{DDA}^+)_{0.028}\text{Au}_{0.06}\text{CsPbBr}_3$ .

The collective optical properties of  $\text{CsPbBr}_3$  supercrystals were also studied with the variation of amount of DDAB– $\text{AuBr}_3$  added to the suspension. Figure 4a shows the UV–vis absorption spectra of  $\text{CsPbBr}_3$  nanocubes before and after the addition of

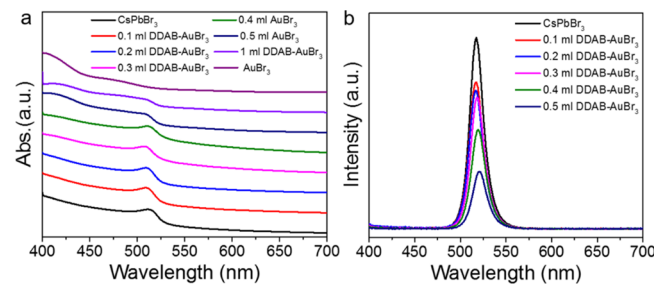


**Figure 4.** (a) UV–vis absorption spectra of as-synthesized  $\text{CsPbBr}_3$  nanocubes and assembled  $\text{CsPbBr}_3$  nanocubes with the addition of different amount of DDAB– $\text{AuBr}_3$  solution and the pure DDAB– $\text{AuBr}_3$  solution. (b) PL emission spectra of as-synthesized  $\text{CsPbBr}_3$  nanocubes and assembled  $\text{CsPbBr}_3$  nanocubes with the addition of different amount of DDAB– $\text{AuBr}_3$  solution.

a different amount of DDAB– $\text{AuBr}_3$  solution. It is obvious that the optical absorption edge around 512 nm changed from sharp to flat and the extended tail absorption appeared, which indicates the variation of the electronic density of states of  $\text{CsPbBr}_3$  nanocubes probably caused by Au–Br complexes or aggregation of nanocubes. In addition, when the amount of DDAB– $\text{AuBr}_3$  solution increased to 0.5 and 1 mL, a broad absorption peak around 420 nm appeared, which is consistent with the absorption peak of DDAB– $\text{AuBr}_3$ , indicating the existence of Au–Br complexes in the supercrystals. The PL spectra of  $\text{CsPbBr}_3$  nanocubes of different status were also collected and plotted in Figure 4b. The emission peak at 517 nm of  $\text{CsPbBr}_3$  nanocubes and  $\text{CsPbBr}_3$  supercrystals exhibits no evident shift following the addition of DDAB– $\text{AuBr}_3$  solution, which indicates that the assembly process would not change the band gap of  $\text{CsPbBr}_3$  nanocubes. However, an obvious decrease in the absolute PL quantum yield (PLQY) was observed, namely, from 37 to 5% (Figure S14), with the increase in amount of DDAB– $\text{AuBr}_3$  solution from 0 to 0.5 mL, due to the quenching effect of the assembly of  $\text{CsPbBr}_3$  nanocubes on their PL. The variation of collective optical properties of assembled  $\text{CsPbBr}_3$  supercrystals interestingly related to the electron transfer from the conducting band of  $\text{CsPbBr}_3$  nanoparticles to the surface trap states induced by the Au–Br complex, and we explore their potentials for photocatalysis.

It is well known that the 3D supercrystals are relatively easier to be disassembled if they are generated by entropic or van der Waals interactions. However, our obtained  $\text{CsPbBr}_3$  supercrystals induced by Au–Br complexes are stable and could maintain the mesostructure after a heating treatment at 80 °C for 30 min (Figure 5a). High-resolution TEM image (Figure 5b) further shows that the  $\text{CsPbBr}_3$  nanocubes fused together via the oriented attachment of (100) crystal planes, indicating the inherently reactive ionic surfaces of  $\text{CsPbBr}_3$  nanocubes. The absence of Au in the heat-treated  $\text{CsPbBr}_3$  mesocrystals was further confirmed by the EDS mapping analysis (Figure 5c–h), implying that Au–Br complexes were excluded by the fusion of  $\text{CsPbBr}_3$  nanocubes under the oriented attachment effect. Moreover, the Au element was also hard to be detected by XPS after the heat treatment (Figure S15), and the Br 3d core level for heat-treated  $\text{CsPbBr}_3$  supercrystals can only be fitted into two peaks at 69.0 and 68.0 eV due to the exclusion out of Au by the transformation of supercrystals to mesocrystals. The UV–vis absorption and PL emission intensity of  $\text{CsPbBr}_3$  supercrystals (Figure S16) were further suppressed due to the growth of  $\text{CsPbBr}_3$  nanocubes into mesocrystals.

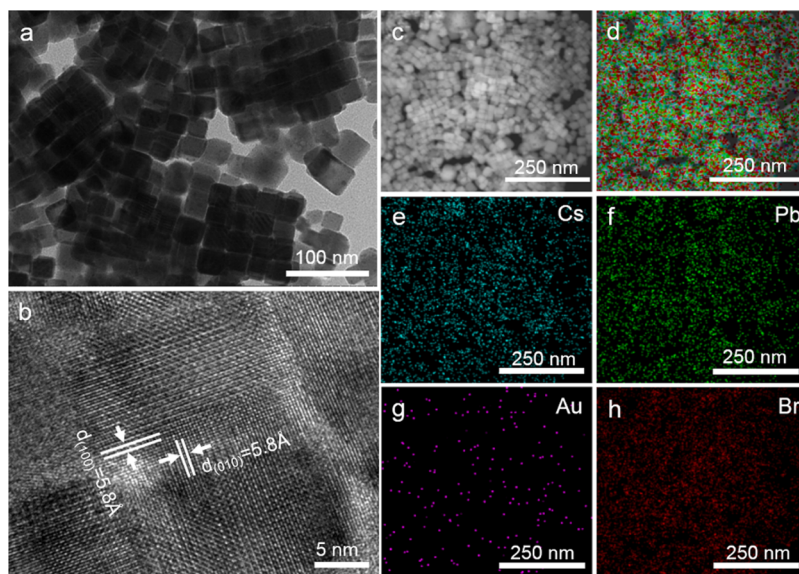


**Figure 5.** (a) TEM image, (b) HRTEM image, and (c) HAADF-STEM image of the assembled  $\text{CsPbBr}_3$  nanocubes after the heating treatment. (d) Overlapped EDS mapping image. (e–h) Corresponding elementary mapping of Cs, Pb, Br, and Au, respectively.

## CONCLUSIONS

We reported novel  $\text{CsPbBr}_3$  supercrystals generated by the van der Waals interactions among carbon chains and electrostatic forces between Au–Br complexes and surfactants to induce the anisotropic assembly of  $\text{CsPbBr}_3$  nanocubes. Through tuning the amount of Au–Br complexes during the assembly process, 2D square-arrays and 3D cubic supercrystals of  $\text{CsPbBr}_3$  nanocubes are obtained, indicating the important role of Au–Br complexes on the assembly. Moreover, the obtained  $\text{CsPbBr}_3$  supercrystal is stable and tends to form the mesocrystal via the oriented attachment growth. With the formation of supercrystal or mesocrystal, the optical properties of  $\text{CsPbBr}_3$  nanocubes are intensively suppressed. This new type of  $\text{CsPbBr}_3$  supercrystal will offer an alternative insight into the exploration of attractive metal halide perovskite nanomaterials.

## ASSOCIATED CONTENT

### Supporting Information

The Supporting Information is available free of charge on the ACS Publications website at DOI: [10.1021/acs.langmuir.7b03432](https://doi.org/10.1021/acs.langmuir.7b03432).

Figure S1. PL emission spectra of as-synthesized  $\text{CsPbBr}_3$  nanocubes and ligand-exchanged  $\text{CsPbBr}_3$  nanocubes. Figure S2. PXRD pattern of as-synthesized  $\text{CsPbBr}_3$  nanocubes and the assembled  $\text{CsPbBr}_3$  supercrystals. Figure S3. TEM image of  $\text{CsPbBr}_3$  nanocubes with the addition of DDAB–AuBr<sub>3</sub> solution in the molar ratio of DDAB. Figure S4. Variation of average size of the assembled  $\text{CsPbBr}_3$  supercrystals with the increase in the amount of DDAB–AuBr<sub>3</sub> solution. Figure S5. TEM image of as-synthesized  $\text{CsPbBr}_3$  nanocubes with larger size and single particle size variation of  $\text{CsPbBr}_3$  nanocubes after addition of DDAB–AuBr<sub>3</sub> solution. Figure S6. TEM image of as-synthesized  $\text{CsPbBr}_3$  nanocubes with smaller size and TEM images of the assembled  $\text{CsPbBr}_3$  nanocubes with the addition of different amount of DDAB–AuBr<sub>3</sub> solution. Figure S7. TEM image of  $\text{CsPbBr}_3$  nanocubes with the addition of only DDAB solution after the ligand exchange. Figure S8. XPS spectra of  $\text{CsPbBr}_3$  nanocubes for the Cs (3d), Pb (4f), and Br (3d). Figure S9.

<sup>1</sup>H NMR reference spectrum of ODE, oleic acid, oleylamine, and DDAB. Figure S10. <sup>1</sup>H NMR spectrum of  $\text{CsPbBr}_3$  nanocubes. Figure S11. <sup>1</sup>H NMR spectrum of assembled  $\text{CsPbBr}_3$  with addition of 0.5 mL of DDAB–AuBr<sub>3</sub> solution. Figure S12. <sup>1</sup>H NMR spectrum of assembled  $\text{CsPbBr}_3$  with addition of 1 mL of DDAB–AuBr<sub>3</sub> solution. Figure S13. TGA curves of assembled  $\text{CsPbBr}_3$  with addition of 1 mL of DDAB–AuBr<sub>3</sub> solution. Figure S14. Plot of PLQY variation of the assembled  $\text{CsPbBr}_3$  nanocubes with different amount of DDAB–AuBr<sub>3</sub> solution added to the  $\text{CsPbBr}_3$  nanocube suspension. Figure S15. XPS spectra of assembled  $\text{CsPbBr}_3$  nanocubes after the heating treatment for the Cs (3d), Pb (4f), Br (3d), and Au (4f). Figure S16. UV–vis absorption spectra and PL emission spectra of the assembled  $\text{CsPbBr}_3$  nanocubes before and after the heating treatment. Table S1. Summary of the zeta potential of as-synthesized  $\text{CsPbBr}_3$  nanocubes, ligand-exchanged  $\text{CsPbBr}_3$  nanocubes, and assembled  $\text{CsPbBr}_3$  supercrystals. ([PDF](#))

## AUTHOR INFORMATION

### Corresponding Authors

\*H.-B.Y.: E-mail: [yhb@ustc.edu.cn](mailto:yhb@ustc.edu.cn).

\*S.-H.Y.: E-mail: [shyu@ustc.edu.cn](mailto:shyu@ustc.edu.cn).

### ORCID

Hong-Bin Yao: [0000-0002-2901-0160](https://orcid.org/0000-0002-2901-0160)

Shu-Hong Yu: [0000-0003-3732-1011](https://orcid.org/0000-0003-3732-1011)

### Notes

The authors declare no competing financial interest.

## ACKNOWLEDGMENTS

We acknowledge the funding support from the National Natural Science Foundation of China (Grants 51571184, 21431006, 21501165, 21573203, 91645202), the Foundation for Innovative Research Groups of the National Natural Science Foundation of China (Grant 21521001), Key Research Program of Frontier Sciences, CAS (Grant QYZDJ-SSW-SLH036), the National Basic Research Program of China (Grant 2014CB931800), and the Users with Excellence and Scientific Research Grant of Hefei Science Center of CAS (2015HSC-UE007).

## ■ REFERENCES

- (1) Talapin, D. V.; Murray, C. B. PbSe nanocrystal solids for n- and p-channel thin film field-effect transistors. *Science* **2005**, *310* (5745), 86–89.
- (2) Coe, S.; Woo, W. K.; Bawendi, M.; Bulovic, V. Electroluminescence from single monolayers of nanocrystals in molecular organic devices. *Nature* **2002**, *420* (6917), 800–803.
- (3) Maier, S. A.; Kik, P. G.; Atwater, H. A.; Meltzer, S.; Harel, E.; Koel, B. E.; Requicha, A. A. G. Local detection of electromagnetic energy transport below the diffraction limit in metal nanoparticle plasmon waveguides. *Nat. Mater.* **2003**, *2* (4), 229–232.
- (4) Sun, S. H.; Murray, C. B.; Weller, D.; Folks, L.; Moser, A. Monodisperse FePt nanoparticles and ferromagnetic FePt nanocrystal superlattices. *Science* **2000**, *287* (5460), 1989–1992.
- (5) Ye, X. C.; Collins, J. E.; Kang, Y. J.; Chen, J.; Chen, D. T. N.; Yodh, A. G.; Murray, C. B. Morphologically controlled synthesis of colloidal upconversion nanophosphors and their shape-directed self-assembly. *Proc. Natl. Acad. Sci. U. S. A.* **2010**, *107* (52), 22430–22435.
- (6) Ye, X. C.; Chen, J.; Engel, M.; Millan, J. A.; Li, W. B.; Qi, L.; Xing, G. Z.; Collins, J. E.; Kagan, C. R.; Li, J.; Glotzer, S. C.; Murray, C. B. Competition of shape and interaction patchiness for self-assembling nanoplates. *Nat. Chem.* **2013**, *5* (6), 466–473.
- (7) Ye, X. C.; Chen, J.; Irrgang, M. E.; Engel, M.; Dong, A. G.; Glotzer, S. C.; Murray, C. B. Quasicrystalline nanocrystal superlattice with partial matching rules. *Nat. Mater.* **2016**, *16* (2), 214–219.
- (8) Bodnarchuk, M. I.; Kovalenko, M. V.; Heiss, W.; Talapin, D. V. Energetic and Entropic Contributions to Self-Assembly of Binary Nanocrystal Superlattices: Temperature as the Structure-Directing Factor. *J. Am. Chem. Soc.* **2010**, *132* (34), 11967–11977.
- (9) Bian, K. F.; Wang, Z. W.; Hanrath, T. Comparing the Structural Stability of PbS Nanocrystals Assembled in fcc and bcc Superlattice Allotropes. *J. Am. Chem. Soc.* **2012**, *134* (26), 10787–10790.
- (10) Shevchenko, E. V.; Talapin, D. V.; Kotov, N. A.; O'Brien, S.; Murray, C. B. Structural diversity in binary nanoparticle superlattices. *Nature* **2006**, *439* (7072), 55–9.
- (11) Yang, H. J.; He, S. Y.; Chen, H. L.; Tuan, H. Y. Monodisperse Copper Nanocubes: Synthesis, Self-Assembly, and Large-Area Dense-Packed Films. *Chem. Mater.* **2014**, *26* (5), 1785–1793.
- (12) Chen, M.; Kim, J.; Liu, J. P.; Fan, H. Y.; Sun, S. H. Synthesis of FePt nanocubes and their oriented self-assembly. *J. Am. Chem. Soc.* **2006**, *128* (22), 7132–7133.
- (13) Zhang, J.; Fang, J. Y. A General Strategy for Preparation of Pt 3d-Transition Metal (Co, Fe, Ni) Nanocubes. *J. Am. Chem. Soc.* **2009**, *131* (51), 18543–18547.
- (14) Dumestre, F.; Chaudret, B.; Amiens, C.; Renaud, P.; Fejes, P. Superlattices of iron nanocubes synthesized from Fe[N(SiMe<sub>3</sub>)<sub>2</sub>]<sub>2</sub>. *Science* **2004**, *303* (5659), 821–823.
- (15) Ahniyaz, A.; Sakamoto, Y.; Bergstrom, L. Magnetic field-induced assembly of oriented superlattices from maghemite nanocubes. *Proc. Natl. Acad. Sci. U. S. A.* **2007**, *104* (45), 17570–17574.
- (16) Shen, X. S.; Wang, G. Z.; Hong, X.; Zhu, W. Simple-cubic microcubes assembled by palladium nanocubes. *CrystEngComm* **2009**, *11* (5), 753–755.
- (17) Rycenga, M.; McLellan, J. M.; Xia, Y. N. Controlling the assembly of silver nanocubes through selective functionalization of their faces. *Adv. Mater.* **2008**, *20* (12), 2416–2420.
- (18) Quan, Z. W.; Xu, H. W.; Wang, C. Y.; Wen, X. D.; Wang, Y. X.; Zhu, J. L.; Li, R. P.; Sheehan, C. J.; Wang, Z. W.; Smilgies, D. M.; Luo, Z. P.; Fang, J. Y. Solvent-Mediated Self-Assembly of Nanocube Superlattices. *J. Am. Chem. Soc.* **2014**, *136* (4), 1352–1359.
- (19) Bishop, K. J. M.; Wilmer, C. E.; Soh, S.; Grzybowski, B. A. Nanoscale Forces and Their Uses in Self-Assembly. *Small* **2009**, *5* (14), 1600–1630.
- (20) Min, Y. J.; Akbulut, M.; Kristiansen, K.; Golan, Y.; Israelachvili, J. The role of interparticle and external forces in nanoparticle assembly. *Nat. Mater.* **2008**, *7* (7), 527–538.
- (21) Song, J.; Li, J.; Li, X.; Xu, L.; Dong, Y.; Zeng, H. Quantum Dot Light-Emitting Diodes Based on Inorganic Perovskite Cesium Lead Halides (CsPbX<sub>3</sub>). *Adv. Mater.* **2015**, *27* (44), 7162–7167.
- (22) Shen, H. B.; Cao, W. R.; Shewmon, N. T.; Yang, C. C.; Li, L. S.; Xue, J. G. High-Efficiency, Low Turn-on Voltage Blue-Violet Quantum-Dot-Based Light-Emitting Diodes. *Nano Lett.* **2015**, *15* (2), 1211–1216.
- (23) Yang, Y. X.; Zheng, Y.; Cao, W. R.; Titov, A.; Hyvonen, J.; Manders, J. R.; Xue, J. G.; Holloway, P. H.; Qian, L. High-efficiency light-emitting devices based on quantum dots with tailored nanostructures. *Nat. Photonics* **2015**, *9* (4), 259–266.
- (24) Zhang, Y.; Xie, C. A.; Su, H. P.; Liu, J.; Pickering, S.; Wang, Y. Q.; Yu, W. W.; Wang, J. K.; Wang, Y. D.; Hahm, J. I.; Dellas, N.; Mohney, S. E.; Xu, J. A. Employing Heavy Metal-Free Colloidal Quantum Dots in Solution-Processed White Light-Emitting Diodes. *Nano Lett.* **2011**, *11* (2), 329–332.
- (25) Dou, L. T.; Wong, A. B.; Yu, Y.; Lai, M. L.; Kornienko, N.; Eaton, S. W.; Fu, A.; Bischak, C. G.; Ma, J.; Ding, T. N.; Ginsberg, N. S.; Wang, L. W.; Alivisatos, A. P.; Yang, P. D. Atomically thin two-dimensional organic-inorganic hybrid perovskites. *Science* **2015**, *349* (6255), 1518–1521.
- (26) Kim, Y.; Yassitepe, E.; Voznyy, O.; Comin, R.; Walters, G.; Gong, X. W.; Kanjanaboos, P.; Nogueira, A. F.; Sargent, E. H. Efficient Luminescence from Perovskite Quantum Dot Solids. *ACS Appl. Mater. Interfaces* **2015**, *7* (45), 25007–25013.
- (27) Schmidt, L. C.; Pertegas, A.; Gonzalez-Carrero, S.; Malinkiewicz, O.; Agouram, S.; Espallargas, G. M.; Bolink, H. J.; Galian, R. E.; Perez-Prieto, J. Non-template Synthesis of CH<sub>3</sub>NH<sub>3</sub>PbBr<sub>3</sub> Perovskite Nanoparticles. *J. Am. Chem. Soc.* **2014**, *136* (3), 850–853.
- (28) Protesescu, L.; Yakunin, S.; Bodnarchuk, M. I.; Krieg, F.; Caputo, R.; Hendon, C. H.; Yang, R. X.; Walsh, A.; Kovalenko, M. V. Nanocrystals of Cesium Lead Halide Perovskites (CsPbX<sub>3</sub>, X = Cl, Br, and I): Novel Optoelectronic Materials Showing Bright Emission with Wide Color Gamut. *Nano Lett.* **2015**, *15* (6), 3692–3696.
- (29) Zhang, D. D.; Eaton, S. W.; Yu, Y.; Dou, L. T.; Yang, P. D. Solution-Phase Synthesis of Cesium Lead Halide Perovskite Nanowires. *J. Am. Chem. Soc.* **2015**, *137* (29), 9230–9233.
- (30) Zhang, F.; Zhong, H. Z.; Chen, C.; Wu, X. G.; Hu, X. M.; Huang, H. L.; Han, J. B.; Zou, B. S.; Dong, Y. P. Brightly Luminescent and Color-Tunable Colloidal CH<sub>3</sub>NH<sub>3</sub>PbX<sub>3</sub> (X = Br, I, Cl) Quantum Dots: Potential Alternatives for Display Technology. *ACS Nano* **2015**, *9* (4), 4533–4542.
- (31) Eaton, S. W.; Lai, M. L.; Gibson, N. A.; Wong, A. B.; Dou, L. T.; Ma, J.; Wang, L. W.; Leone, S. R.; Yang, P. D. Lasing in robust cesium lead halide perovskite nanowires. *Proc. Natl. Acad. Sci. U. S. A.* **2016**, *113* (8), 1993–1998.
- (32) Protesescu, L.; Yakunin, S.; Bodnarchuk, M. I.; Bertolotti, F.; Masciocchi, N.; Guagliardi, A.; Kovalenko, M. V. Monodisperse Formamidinium Lead Bromide Nanocrystals with Bright and Stable Green Photoluminescence. *J. Am. Chem. Soc.* **2016**, *138* (43), 14202–14205.
- (33) Wang, K. H.; Wu, L.; Li, L.; Yao, H. B.; Qian, H. S.; Yu, S. H. Large-Scale Synthesis of Highly Luminescent Perovskite-Related CsPb<sub>2</sub>Br<sub>5</sub> Nanoplatelets and Their Fast Anion Exchange. *Angew. Chem., Int. Ed.* **2016**, *55* (29), 8328–8332.
- (34) Nedelcu, G.; Protesescu, L.; Yakunin, S.; Bodnarchuk, M. I.; Grotevent, M. J.; Kovalenko, M. V. Fast Anion-Exchange in Highly Luminescent Nanocrystals of Cesium Lead Halide Perovskites (CsPbX<sub>3</sub>, X = Cl, Br, I). *Nano Lett.* **2015**, *15* (8), 5635–5640.
- (35) Akkerman, Q. A.; D'Innocenzo, V.; Accornero, S.; Scarpellini, A.; Petrozza, A.; Prato, M.; Manna, L. Tuning the Optical Properties of Cesium Lead Halide Perovskite Nanocrystals by Anion Exchange Reactions. *J. Am. Chem. Soc.* **2015**, *137* (32), 10276–10281.
- (36) Zhang, D. D.; Yang, Y. M.; Bekenstein, Y.; Yu, Y.; Gibson, N. A.; Wong, A. B.; Eaton, S. W.; Kornienko, N.; Kong, Q.; Lai, M. L.; Alivisatos, A. P.; Leone, S. R.; Yang, P. D. Synthesis of Composition Tunable and Highly Luminescent Cesium Lead Halide Nanowires through Anion-Exchange Reactions. *J. Am. Chem. Soc.* **2016**, *138* (23), 7236–7239.
- (37) Nagaoka, Y.; Hills-Kimball, K.; Tan, R.; Li, R.; Wang, Z.; Chen, O. Nanocube Superlattices of Cesium Lead Bromide Perovskites and

Pressure-Induced Phase Transformations at Atomic and Mesoscale Levels. *Adv. Mater.* **2017**, *29* (18), 1606666.

(38) Bekenstein, Y.; Koscher, B. A.; Eaton, S. W.; Yang, P. D.; Alivisatos, A. P. Highly Luminescent Colloidal Nanoplates of Perovskite Cesium Lead Halide and Their Oriented Assemblies. *J. Am. Chem. Soc.* **2015**, *137* (51), 16008–16011.

(39) Li, X. M.; Wu, Y.; Zhang, S. L.; Cai, B.; Gu, Y.; Song, J. Z.; Zeng, H. B.  $\text{CsPbX}_3$  Quantum Dots for Lighting and Displays: Room-Temperature Synthesis, Photoluminescence Superiorities, Underlying Origins and White Light-Emitting Diodes. *Adv. Funct. Mater.* **2016**, *26* (15), 2435–2445.

(40) Pan, J.; Quan, L. N.; Zhao, Y. B.; Peng, W.; Murali, B.; Sarmah, S. P.; Yuan, M. J.; Sinatra, L.; Alyami, N. M.; Liu, J. K.; Yassitepe, E.; Yang, Z. Y.; Voznyy, O.; Comin, R.; Hedhili, M. N.; Mohammed, O. F.; Lu, Z. H.; Kim, D. H.; Sargent, E. H.; Bakr, O. M. Highly Efficient Perovskite-Quantum-Dot Light-Emitting Diodes by Surface Engineering. *Adv. Mater.* **2016**, *28* (39), 8718–8725.